

PACS numbers: 42.79.Kr; 42.79.Hp
DOI: 10.1070/QE2011v041n01ABEH014407

Tunable liquid-crystal focusing device. 2. Experiment

S.P. Kotova, V.V. Patlan, S.A. Samagin

Abstract. **The characteristics of a modal liquid-crystal focusing device are experimentally investigated in different control regimes. Phase delay distributions in the form of a circular truncated cone with a controlled position of the base centre are obtained. Focusing to a round spot with a controlled position of the focal point in the aperture area is implemented for the focusing device operation in the regime of a small modal parameter.**

Keywords: *liquid crystals, spatial light modulators.*

1. Introduction

The theoretical modelling of the operation of a liquid-crystal (LC) focusing device based on crossed substrates with a resistive coating and stripe contacts [1] showed its applicability for implementing some phase distributions of practical interest. The operation of a two-dimensional LC deflector (which is similar to the device under study), at a small modal parameter, was considered in [2, 3]. A set of optical elements with a complex phase delay profile was realised in [3]; however, there was no detailed theoretical description of the control regime and the problem of light focusing was not analysed. In this context, the control regimes found by us in [1] are new. Here, we experimentally studied the aforementioned focusing device, implemented some new operation regimes, and considered their application for controlled light focusing.

2. Experimental samples of focusing devices

We prepared samples of tunable LC focusing devices with square apertures of three sizes; the aperture sides were 1, 2, and 5 mm long. The focusing device design is schematically shown in Fig. 1. The high-resistivity coatings on both substrates of each focusing device had equal surface resistances (100 kΩ$\square^{-1}$ and 5 MΩ$\square^{-1}$ for different samples). The LC layer thickness (set by Teflon spacers) was 10 or 12.5 μm. BL037 nematic (Merck) was used in the focusing devices. Planar orientation of the LC layer was set using orienting coatings.

To study the characteristics of the modal focusing device, we designed and fabricated a special computer-aided quad-channel sine-wave generator, based on integrated circuits: a

S.P. Kotova, V.V. Patlan, S.A. Samagin Samara Branch of the P.N. Lebedev Physics Institute, Russian Academy of Sciences, Novo-Sadovaya ul. 221, 443011 Samara, Russia;
e-mail: kotova@fian.smr.ru

Received 28 July 2010; revision received 1 November 2010
Kvantovaya Elektronika **41** (1) 65–70 (2011)
Translated by Yu.P. Sin'kov

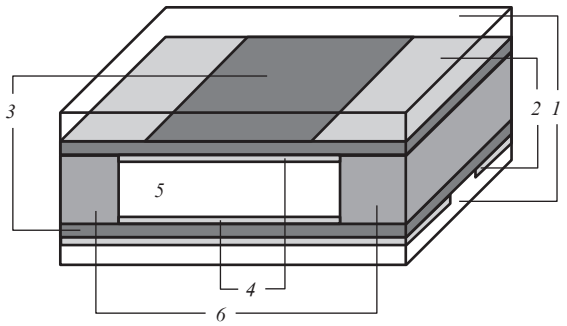

Figure 1. Schematic diagram of LC focusing device: (*1*) glass substrates, (*2*) low-resistivity electrodes, (*3*) high-resistivity conducting layer, (*4*) orienting coating, (*5*) LC layer, and (*6*) spacers.

12-bit digital-to-analogue converter DAC7615P and microcontroller PIC18F252. Direct digital synthesis was implemented using the table of sine values, stored in the nonvolatile memory of the microcontroller. The values from the table are chosen by a microprogram every cycle, separated by equal specified time intervals, according to the current value of the phase counter, scaled to obtain a desired amplitude with hardware implemented multiplication and bitwise shift, and then loaded to the DAC through SPI (Serial Peripheral Interface). The thus formed sinusoidal signal with an amplitude up to 2.5 V, zero-biased (due to the DAC design features), is converted to a zero-symmetric signal with an amplitude up to 12.5 V by an operational amplifier (OA) TL074. The microcontroller (operating at a clock frequency of 50 MHz) provides up to 64 counts per period for a voltage frequency of 500 Hz, which is sufficient to carry out the experiments planned. The data from the computer are transferred through a standard serial interface RS-232C; the electric signal amplitude and phase shift are set independently for each of the four channels only at a variation in these parameters. The control software, implemented in a personal computer, has a simple and convenient graphical interface, which imitates the panel board of the virtual device.

The phase delay profile of the LC focusing device was investigated by standard techniques in a scheme with crossed polaroids (Fig. 2). Samples were placed between crossed polaroids so as to provide an angle of 45° between the direction of the initial orientation of the LC layer optical axis and the polaroid axes. The LC focusing device was illuminated by a uniform linearly polarised He–Ne laser beam with a plane wavefront and a wavelength of 633 nm. Potentials (calculated from the relations obtained for different focusing device operation regimes) were applied to the contact electrodes.

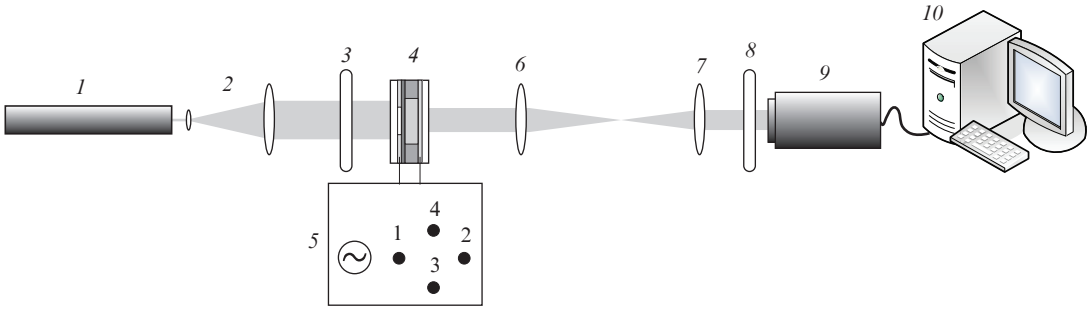

Figure 2. Schematic diagram of polarisation interferometer for visualising the phase delay of LC focusing device: (*1*) He–Ne laser, (*2*) collimator, (*3*) polaroid, (*4*) LC focusing device, (*5*) control unit, (*6*, *7*) lenses, (*8*) polaroid, (*9*) CCD camera, (*10*) computer.

3. Operation of the LC focusing device at different values of the modal parameter

As was noted in [1], the modal control regime is implemented at a modal parameter $|\chi| \sim 1/l$, where l is the aperture size. The modal parameter can be controlled by changing the frequency of the applied voltage during operation. The electrical characteristics of the device elements (in particular, the surface resistance of high-resistivity coatings) were chosen so as to match the voltage frequencies with the LC operating range.

Identical in-phase potentials φ_1 and φ_2 were applied to the contacts of one of the substrates, while the contacts on the other substrate were grounded. The interference patterns obtained in this control regime are shown in Fig. 3. It can clearly be

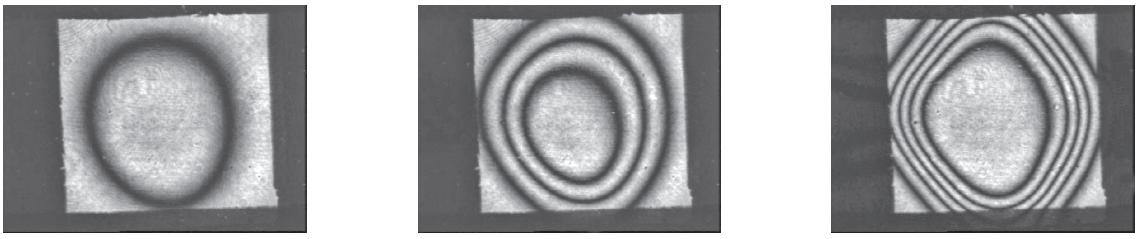

Figure 3. Interference patterns obtained in the scheme with crossed polaroids, for a focusing device with an aperture of 5×5 mm, at a voltage amplitude of 10 V and frequencies of (a) 0.4, (b) 0.7, and (c) 1.5 kHz.

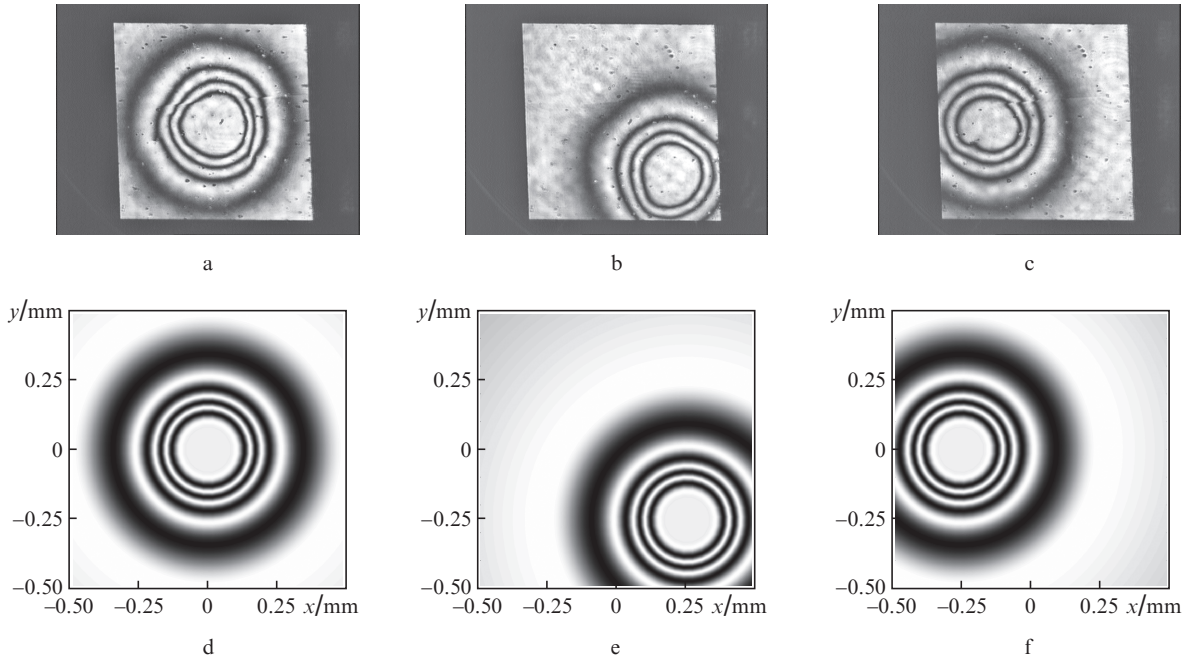

Figure 4. (a–c) Experimental and (d–f) calculated interference patterns for an LC focusing device operating in the regime of a small modal parameter. The centre coordinates are (a, d) $x_0/a = y_0/b = 0$; (b, e) $x_0/a = 0.5$, $y_0/b = -0.5$; and (c, f) $x_0/a = 0.5$, $y_0/b = 0$.

seen that an increase in the voltage frequency leads to an increase in the depth of the phase delay profile, and the influence of the geometry of the contact electrodes forming the aperture also increases. Obviously, this operation regime is not optimal for focusing, and one should use the potential frequency range in which the modal parameter is small.

Within the mathematical model of the focusing device [1] we obtained solutions for a small modal parameter, i.e., for the case where the condition $|\chi\lambda| \ll 1$ is satisfied. This inequality is valid for experimental samples of focusing devices with the apertures of 1×1 and 2×2 mm. Their operation was similar; therefore, we report only the experimental data for the focusing device with the aperture of 1×1 mm as illustrated below.

The experimental results in Fig. 4 confirm the validity of the relations [1] for calculating the control potentials in the case where two potentials are initially set: $\varphi_{11} = 4.24$ V and $\varphi_{12} = (-2.5–4.33\mathrm{i})$ V. The others were calculated using relations (12) [1].

The solution with fixed potential phases (expression (14) in [1]) is the simplest to be implemented in practice and determine the control signals, because it is only the potential amplitudes that change; moreover, three of them unambiguously depend on the fourth one. Let us consider the experimental realisation of this approach. The experimental characteristic interference patterns are shown in Fig. 5. The potentials were calculated from formulas (14) and (18) [1], using the parameter values and the experimental voltage–phase dependence for a specific sample. The theoretical and experimental data demonstrated good agreement. Note that when the wavefront distribution with elliptical constant-phase lines is formed, astigmatism arises in the phase delay profile, while it is absent in the patterns shown in Fig. 5.

Since the voltage at the centre of the pattern is zero, an area with a constant phase delay is observed in this region. This is confirmed by the Hartmann sensor measurements of the light wavefront transmitted through the focusing device

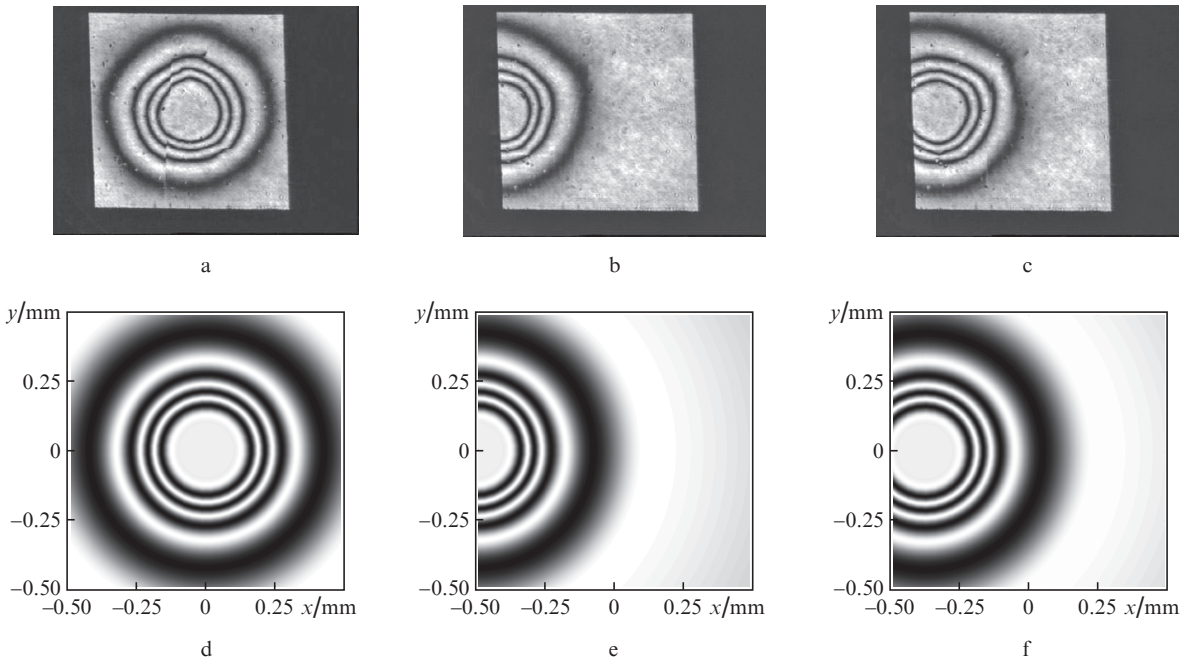

Figure 5. (a–c) Experimental and (d–f) calculated polarisation interference patterns for an LC focusing device with an aperture of 1×1 mm, at a voltage frequency of 500 Hz and effective contact potentials (a, d) $A_{11} = A_{12} = 4$ V; (b, e) $A_{11} = 0$, $A_{12} = 8$ V; and $A_{11} = 1$ V, $A_{12} = 7$ V ($A_{21} = A_{22} = 4$ V in all cases).

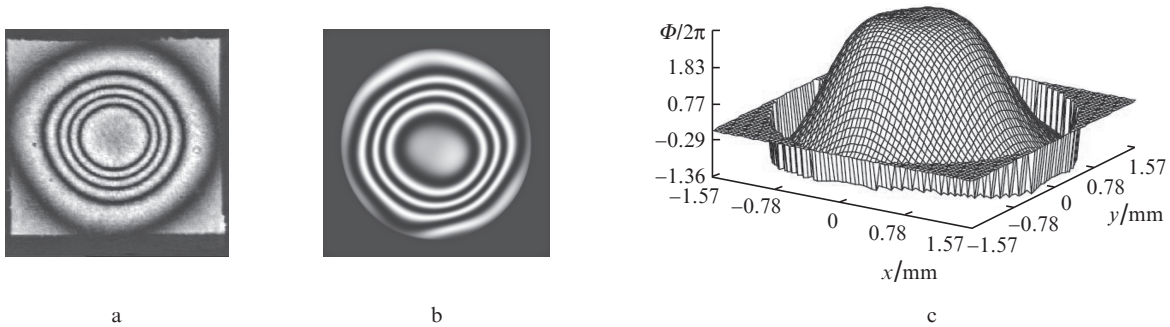

Figure 6. (a) Experimental interference pattern obtained in the scheme with crossed polaroids, (b) the interference pattern calculated from the results of wavefront sensor measurements, and (c) the wavefront for a focusing device with an aperture of 5×5 mm, at a voltage frequency of 100 Hz and a voltage amplitude of 4.0 V. The control regime corresponds to the constant-phase solution.

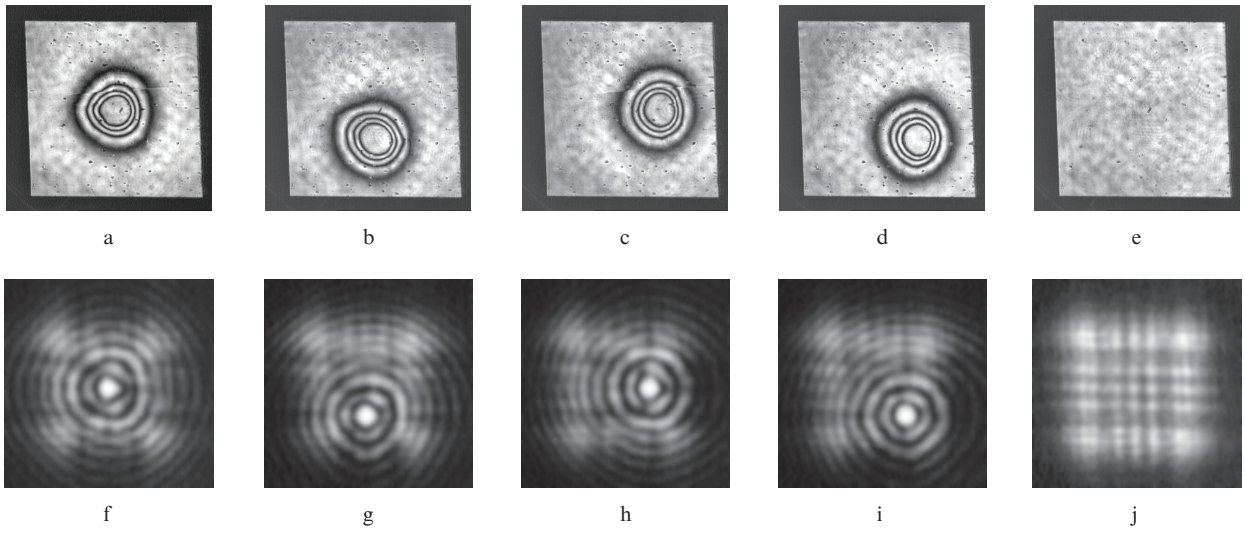

Figure 7. (a–e) Experimental polarisation interference patterns and (f–j) intensity distributions at a distance of 9 cm from the focusing device, obtained for a focusing device with an aperture of 1×1 mm, at a voltage frequency of 500 Hz and contact potential amplitudes (a, f) $A_{11} = A_{22} = A_{12} = A_{21} = 9$ V; (b, g) $A_{11} = A_{12} = 9$ V, $A_{22} = 12$ V, $A_{21} = 6$ V; (c, h) $A_{11} = 12$ V, $A_{22} = A_{21} = 9$ V, $A_{12} = 6$ V; and (d, i) $A_{11} = A_{22} = 12$ V, $A_{12} = A_{21} = 6$ V; (e, j) the focusing device is switched off.

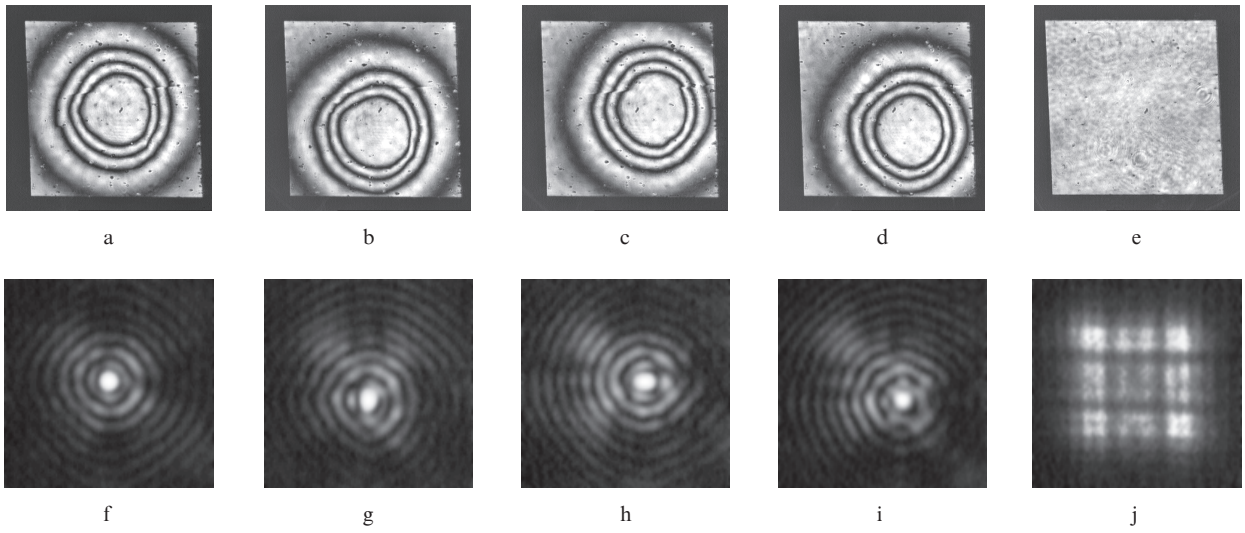

Figure 8. (a–e) Experimental polarisation interference patterns and (f–j) intensity distributions (image size 1.3×1.3 mm) at a distance of 12 cm from the focusing device, obtained for a focusing device with an aperture of 1×1 mm, at a voltage frequency of 500 Hz and contact potential amplitudes (a, f) $A_{11} = A_{22} = A_{12} = A_{21} = 4$ V; (b, g) $A_{11} = A_{12} = 4$ V, $A_{22} = 5$ V, $A_{21} = 3$ V; (c, h) $A_{11} = 5$ V, $A_{22} = A_{21} = 4$ V, $A_{12} = 3$ V; and (d, i) $A_{11} = A_{22} = 5$ V, $A_{12} = A_{21} = 3$ V; (e, j) the focusing device is switched off.

(Fig. 6). The experimental setup is similar to the system for obtaining polarisation interference patterns (Fig. 2), but the second polaroid [(*8*) in Fig. 2] is absent, and camera (*9*) is replaced with a Hartmann sensor. The first polaroid is oriented so as to align its transmission axis with the LC optical axis at zero voltage. The Hartmann array had a hexagonal structure; therefore, the measurements were performed for not the entire aperture but only its central part.

Obviously, if the constant-voltage lines are concentric circles, the transmitted light will be focused to a round spot, which will move on the screen, along with the centre of phase delay distribution (Figs 7, 8). It can clearly be seen that, the higher the potentials, the smaller the aperture area involved in light focusing and, therefore, the lower the radiation power P falling in the focal spot. For example, at a potential amplitude of 9 V (Fig. 7), the power fraction in the spot is 7.5% of the total transmitted light power P_0; at an amplitude of 4 V this fraction increases to 19% (Fig. 8). At the same time, at large voltages the focal spot in the aperture can be displaced within a larger area without any loss of quality. This circumstance is favourable for focusing devices used in systems for manipulating microscopic objects.

Since the wavefront formed is not parabolic but has rather the form of a truncated cone with different base diameters, light focusing in a spot is observed on an extended portion along the light propagation axis. This means that a light intensity distribution in the form of a segment oriented in the longitudinal direction is formed at some distance from the

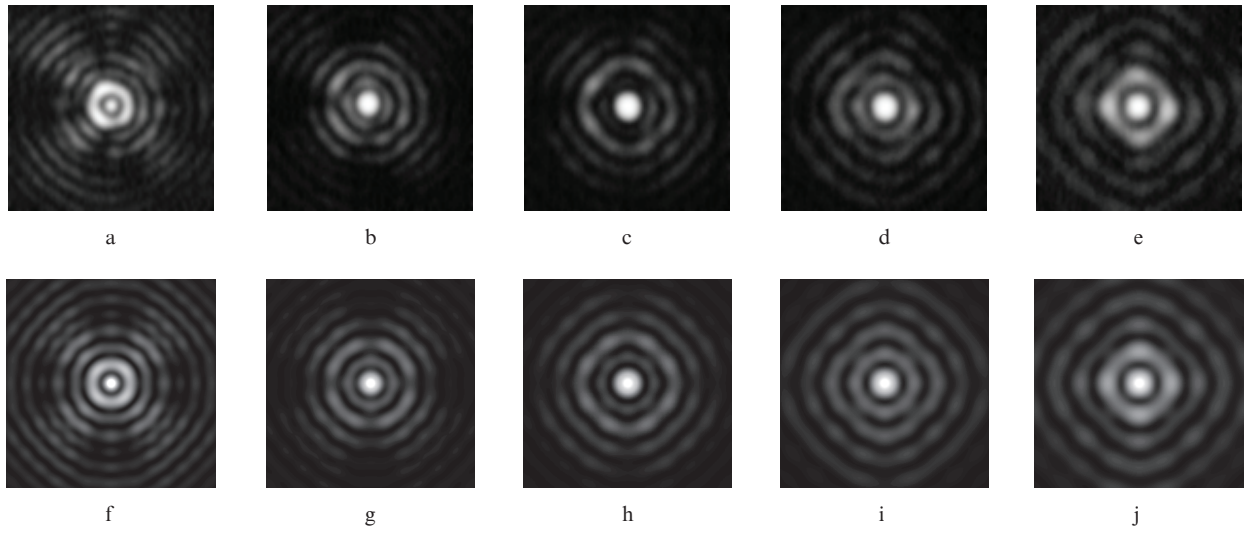

Figure 9. (a–e) Experimental and (f–j) theoretical images of focal spots along the light propagation axis for a focusing device with an aperture of 1×1 mm at a contact potential amplitude of 4 V; a voltage frequency of 500 Hz; and phases $\alpha_{11} = 0$, $\alpha_{22} = 90°$, $\alpha_{12} = 180°$, and $\alpha_{21} = 270°$. The distances from the focusing device are (a, e) 10, (b, f) 12, (c, g) 14, (d, i) 16, and (e, j) 18 cm. All images are 1×1 mm in size.

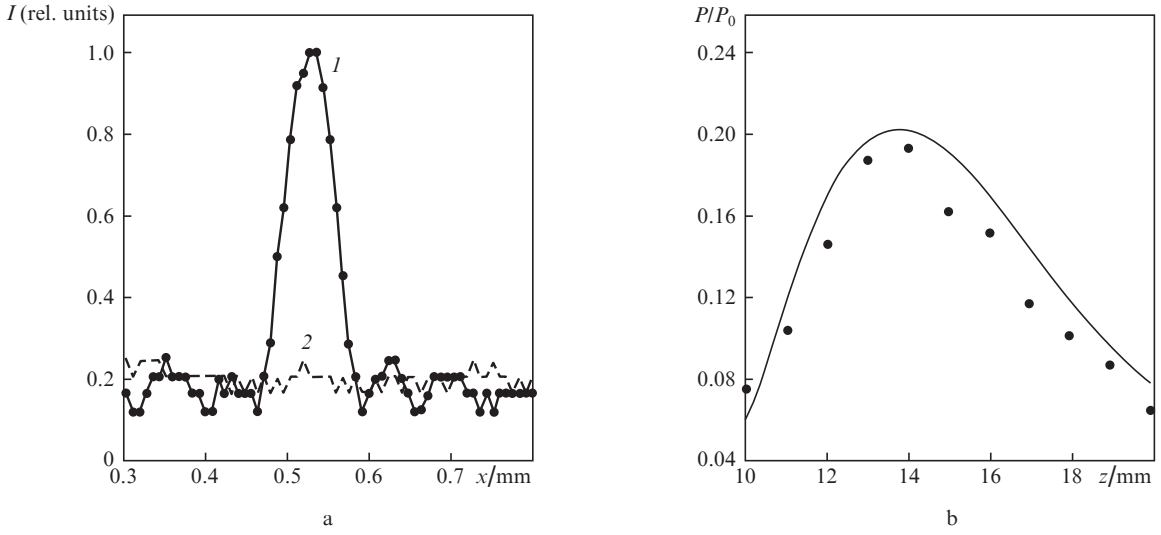

Figure 10. (a) Intensity distributions in the cross section (*1*) for a focusing device with an aperture of 1×1 mm at a contact potential amplitude of 4 V; a voltage frequency of 500 Hz; and phases $\alpha_{11} = 0$, $\alpha_{22} = 90°$, $\alpha_{12} = 180°$, and $\alpha_{21} = 270°$ and (*2*) for the case with a switched-off focusing device (the distance from the focusing device to the screen is 14 cm). (b) The calculated (solid line) and experimental (circles) dependences of the radiation power fraction in the central spot, P/P_0, on the distance.

focusing device. The position of the segment beginning depends on the shape of the cone of the wavefront formed, while its length is determined by the wavefront shape and the effect of diffraction from the aperture edges. An example of such focusing is shown in Fig. 9. The intensity distribution in the screen and the dependence of the light power fraction falling in the central spot on the distance are shown in Fig. 10. When calculating the intensity distribution, we used the Fresnel transform for a phase delay distribution equivalent to the experimental one (Fig. 8a).

A practically important characteristic of such devices is their operating speed. As well as for all LC elements, it is mainly determined by the reorientation rate of LC molecules in an external field. For nematic crystals with a layer thickness of 10 μm the characteristic switching times are generally several tenths of a second. The process of switching on the LC focusing device is shown in Fig. 11 in the form of intensity patterns in the observation plane at different instants, at a distance of 9 cm from the device.

The low operating speed of these devices limits the range of their application; however, the characteristic times of refocusing on the order of a second are sufficient for some problems (for example, control of microscopic objects). Figure 12 shows an example of displacing the focal spot in the observation plane. Voltages were applied to the LC focusing device for only two cases: to focus light at the centre and in a corner. It can be seen that, due to the high LC relaxation time (few seconds), the transition from the first state to the second state occurs continuously, along an almost straight-line trajectory, and without significant deterioration of the focusing quality.

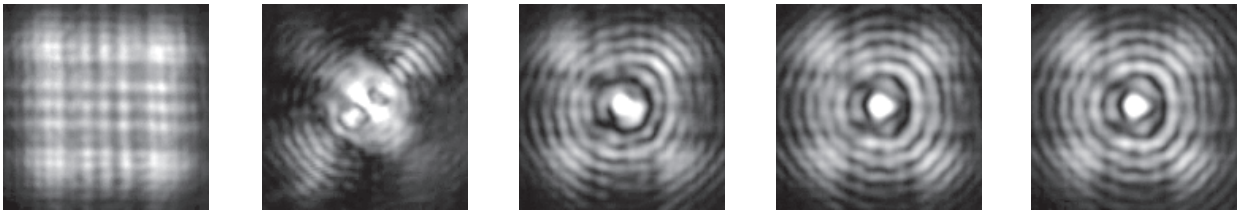

Figure 11. Light intensity distributions at a distance of 9 cm from the focusing device at different instants t after applying potentials.

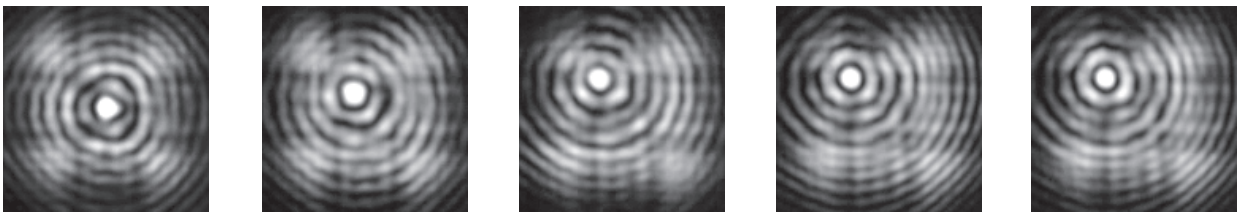

Figure 12. Light intensity distributions at a distance of 9 cm from the focusing device at different instants t during focal spot displacement.

The displacement length was 0.35 mm for 0.68 s, which is acceptable for laser control of microscopic objects.

4. Conclusions

Laboratory samples of LC focusing devices with apertures of 1×1, 2×2, and 5×5 mm and high-resistivity coatings with resistances of 100 kΩ $\square^{-1}$ and 5 MΩ $\square^{-1}$ were developed and fabricated. Different control regimes were experimentally studied. The modulator operation regime corresponding to the case of large modal parameter (regime of modal lens) does not yield any phase delay distributions of practical importance, because a strong dependence on the geometry of aperture edges (which leads to distortions) is observed in all cases. For a small modal parameter (low frequencies and/or low surface resistance of conducting coatings) we obtained phase delay distributions in the form of a circular truncated cone with a controlled position of the base centre. Focusing to a round spot with a controlled position of the focal point in the aperture area was implemented. The experimental data are in good agreement with the model calculations.

Acknowledgements. We are grateful to V.M. Shoshin and Yu.P. Bobylev for their help in fabricating LC focusing devices. This study was supported by the Federal Target Program 'Scientific and Scientific-Pedagogical Personnel of Innovative Russia' for 2009–2013 (State Contract No. 14.740.11.0063).

References

1. Kotova S.P., Patlan' V.V., Samagin S.A. *Kvantovaya Elektron.*, **41**, 58 (2011) [*Quantum Electron.*, **41**, 58 (2011)].
2. Hands Ph.J.W., Tatarkova S.A., Kirby A.K., Love G.D. *Opt. Express*, **14**, 4525 (2006).
3. Kirby A.K., Hands Ph.J.W., Love G.D. *Opt. Express*, **15**, 13496 (2007).